International Journal of Security and Its Applications
Vol. 10, No. 2 (2016), pp.385-410
http://dx.doi.org/10.14257/ijsia.2016.10.2.34

Smartly Time of Arrival Interpretation in the Wide Band Ranging System

Xiaolin Liang[1], Hao Zhang[1, 2], Tingting Lv[1], T. Aaron Gulliver[2]

[1]*College of Information Science and Engineering, Ocean University of China Qingdao, 266100, China;*
[2]*Department of Electrical and Computer Engineering, University of Victoria Victoria, V8W 3P6, Canada*
xiaolin87liang@163.com, zhanghao@ouc.edu.cn
lvtingting33@163.com, agullive@ece.uvic.ca

Abstract

In the field of sensor networks, impulse radio 60 GHz wide band signals which is even much more practical for ranging and localization systems due to high time and multipath resolution. Typically, the 60GHz accurate ranging estimation is very important. In order to improve the precision of the ranging, a new threshold selection algorithm using neural network (NN) is proposed which is based on a joint metric of the skewness, kurtosis and standard deviation after energy detector (ED). Simulation results are presented which show the proposed NN algorithm provides better precision and robustness in both high and low SNR environments than other ED-based algorithms in the IEEE 802.15.3c channel models.

Keywords*: wide band, ranging, IEEE* 802.15.3c

1. Introduction

The demand for high data rate wireless communications with low latency has increased dramatically in recent years. Unfortunately, due to the spectrum limitations and the transmit power regulations, current short-range wireless communication strategies cannot achieve Gigabit per second data rates. Fortunately, wireless communications in the 60GHz millimeter wave band has become viable for Gbps wireless communication networks [1-4] due to the availability of several GHz of license-free spectrum, up to 10W maximum transmit power, no interference from other systems and the development of low-cost complementary metal-oxide semiconductor devices.

The Federal Communications Commission (FCC) permits communications in the 60GHz unlicensed band at an effective isotropic radiated power up to 40dBm, which is many times greater than other short-range wireless communication strategies. In China, this limit is 44dBm [5]. Although the path loss is high at 60GHz, the received power can still be significant. IR communication strategies have been proposed for this frequency band because it can be effective in separating the multipath signals at the receiver. This is because short pulses are employed for communications with a duration (typically under 100 picoseconds), which is far less than the multipath propagation delay. These signals can also provide the fine multipath resolution required for high precision ranging and localization [6]. Thus, 60GHz signals are even much suitable for localization applications for short distances.

Generally, the localization strategies can be classified into time based [7-10] and non-time based [11]. For example, (time of arrival) TOA [10, 12] and (time difference of arrival) TDOA [10] are time based strategies, while the received signal strength (RSS) and angle of arrival (AOA) [11] are non-time based. Localization that based on time is much suitable for using with 60GHz strategy [11], as it can take full advantage of the

ISSN: 1738-9976 IJSIA

higher time and multipath resolution available with very short 60GHz signals. TOA estimation is the key to accurate ranging, but this is very challenging due to the potentially hundreds of multipath components in 60GHz channels, even in the non-line of sight (NLOS) environments.

TOA estimation has been extensively studied [12, 15-18] for the past few years. There are two approaches which are much more applicable for TOA estimation, matched filter (MF) [16] with a higher sampling rate and higher precision correlation, or ED [18] with a lower sampling rate and lower complex. MF is the optimal strategy for TOA estimation, where a correlator template is matched exactly to the received signal. However, a receiver operating at the Nyquist sampling rate makes it very difficult to align with the multipath components of the received signal [15]. In addition, MF requires a priori estimation of the channel, including the timing, fading coefficient, and pulse shape for each component of the impulse response [15]. Because of the high sampling rates and channel estimation, MF may not be practical in many applications. As opposed to MF, ED is a non-coherent approach to TOA estimation. It consists of a square-law device, followed by an integrator, sampler and a decision mechanism. The TOA is made by comparing the integrator output with a threshold and choosing the first sample to exceed the threshold. This is a convenient strategy that directly yields an estimate of the start of the received signal. Thus, a low complexity, low sampling rate receiver can be employed without the need for a priori channel estimation.

The major challenge with ED is the selection of an appropriate threshold based on the received signal samples. NN has extensively been used in signal processing applications. The weights between the input and output layers can be adjusted to minimize the error between the input and output. Because of the complexity of wireless environments, it is difficult to derive a closed-form expression to estimate the TOA. On the other hand, NN can provide a very flexible mapping based on the training input. NN here intends to solve a regression problem.

In this paper, we consider the relationship between the SNR and the statistics of the integrator output including kurtosis, skewness and standard deviation. A metric based on kurtosis, skewness and standard deviation is then developed for threshold selection. The threshold for different SNR values is investigated and the effects of the integration period and channel are examined. Performance results are presented which show that in both the CM1.1 and CM2.1 channels, this joint metric provides higher precision and robustness.

The remainder of this paper is organized as follows. In section 2 the system model is outlined. Section 3 discusses various TOA estimation algorithms based on ED. Section 4 considers the statistical characteristics of the energy values. In section 5 a joint metric based on skewness, kurtosis and standard deviation is proposed. A novel TOA estimation algorithm is introduced based on a NN. Some performance results are presented in section7 and section 8 concludes the paper.

2. System Model

Currently, there are two important standards that have been developed for 60GHz wireless communications systems, IEEE 802.15.3c and IEEE 802.11ad [19-20]. In this paper, the channel models in IEEE 802.15. 3c standard are used because it is specifically designed for Wireless Personal Area Networks and thus encompasses typical indoor environments. Further, these are the most widely employed models for 60GHz systems. IEEE 802.15.3c standard was the first developed for high data rate short-range wireless systems. The physical layer was designed to support the transmission of data within a few meters at a minimum data rate of 2 Gbps. These models have been developed for communications in the frequency band 57 to 66GHz in indoor residential, indoor office and library environments (with differences largely due to the LOS and NLOS characteristics) [21-25]. In this paper, a pulse position modulation time hopping 60GHz

signal is employed for ranging purposes. The propagation delay $\hat{\tau}$, between the transmitter and receiver is estimated for using in localization.

2.1. 60 GHz Signal

The 2PPM-TH-60GHz signals have a very short duration (typically 100 picoseconds or less), and can be expressed as:

$$s(t)=\sum_{-\infty}^{\infty} p\left(t-jT_s-C_jT_c-a_j\varepsilon\right) \tag{1}$$

Each symbol is represented by a sequence of very short pulses, where T_s is the symbol time. The time hopping code represented by C is a pseudorandom integer-valued sequence which is unique for each user to limit multiple access interference, and T_c is the chip time. The PPM time shift is ε so that if a_j is 1, the signal is shifted in time by ε, while a_j is 0, there is no shift. In general, these parameters satisfy the following relationship:

$$(1)C_jT_c+\varepsilon<T_s;(2)\varepsilon<T_c;(3)a_j\varepsilon<C_jT_c\left(C_j\neq 0\right)$$

Many pulse shapes have been proposed for 60GHz systems. In this paper a Gaussian pulse is employed which is multiplied by the carrier signal to give as shown in the Figure1 [26].

$$p(t)=\frac{\sqrt{2}}{\alpha}\exp\left(-2\pi\frac{t^2}{\alpha^2}\right)\cos\left(2\pi f_c t\right) \tag{2}$$

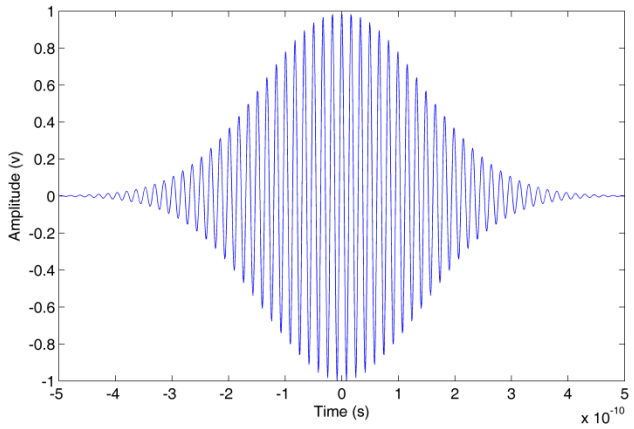

Figure 1. Waveform of the 60GHz Signal

where α is the shape factor, and f_c is the carrier frequency which here is $f_c=60GHz$. A smaller shape factor results in a shorter duration pulse and a larger bandwidth.

2.2. Signal Shift and Path Loss

The path loss is defined as the ratio of the received signal power to the transmit signal power and it is very important for link budget analysis. Unlike narrow-band system, the path loss for a wide-band system such as mm-wave system is both distance and frequency dependent. In order to simplify the models, it is assumed that the frequency dependence Path Loss is negligible and only distance dependence path loss is modeled. The signal path loss, which depends on the propagation distance and the channel (IEEE802.15.3c), is described by:

$$PL(d)[dB]=PL_0+10\cdot n\log_{10}\left(\frac{d}{d_0}\right)+X_\sigma[dB];\ d\geq d_0 \tag{3}$$

where d_0 and d denote the reference distance, and distance respectively. X_σ that the unit is dB, with mean zero and variance σ_s for a Gaussian random variable [11]. The signal shift can be expressed as:

$$t = dt * floor\left(\left(d / c\right)/dt\right) \tag{4}$$

where d denotes the distance between the transmitter and receiver, dt is the sampling period and c is the speed of light which is 299792458 m/s in the air.

2.3. Multipath Fading Channel

The received signal can be written as:

$$r(t) = \sum_{n=1}^{N} \alpha_n p\left(t - \tau_n\right) + n(t) \tag{5}$$

where N is the number of received multipath components, α_n and τ_n denotes the amplitude and delay of the *nth* path respectively, $p(t)$ is the received 60GHz pulse and $n(t)$ is the Additive White Gaussian Noise (AWGN) with zero mean and two sided power spectral density $N_0/2$. Eq. (5) can be rewritten as:

$$r(t) = s(t) * h(t) + n(t) \tag{6}$$

where $s(t)$ is the transmitted signal, and $h(t)$ is the channel impulse response which can be expressed as:

$$h(t,\theta) = \sum_{k=1}^{K} \sum_{l=1}^{L_k} \mu_{kl} \delta\left(t - T_k - \tau_{kl}\right) \delta\left(\theta - \theta_k - \omega_{kl}\right) \tag{7}$$

where $\delta(.)$ is the Dirac delta function, K is the number of clusters, L_k is the number of rays in the k^{th} cluster, and μ_{kl} , τ_{kl} and ω_{kl} denote the complex amplitude, delay and azimuth of the k^{th} ray of the l^{th} cluster, respectively. Similarly, T_k and θ_k represent the delay and mean Angle of Arrival of the k^{th} cluster.

2.4. Energy Detector

As shown in Figure 2 [27], after the amplifier, the received signals are squared, and then input to an integrator with integration period Tb . Because of the inter-frame leakage due to multipath signals, the integration duration is $3T_f / 2$, so the number of signal values for ED is $N = 3T_f / 2Tb$. The integrator outputs can be expressed as:

$$z[n] = \sum_{i=1}^{N} \int_{(i-1)T_f + (c_j + n)Tb}^{(i-1)T_f + (c_j + n-1)Tb} r^2(t) dt \tag{8}$$

where $n \in \{1,2,..,N\}$ denotes the sample index with respect to the starting point of the integration period and N is the number of pulses per symbol. Here, N is set to 1, so the integrator outputs are

$$z[n] = \sum_{i=1}^{N} \int_{(c_j + n-1)Tb}^{(c_j + n)Tb} r^2(t) dt \tag{9}$$

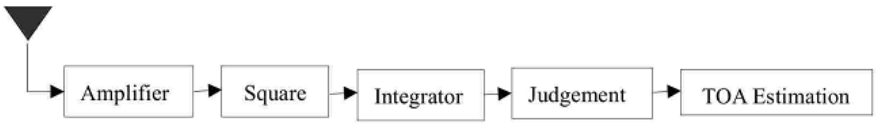

Figure2. Block Diagram of the Energy Detector Receiver

If $z[n]$ is the integration of noise only, it has a centralized Chi-square distribution, while it has a non-centralized Chi-square distribution if a signal is present. The mean and

variance of the noise and signal values are given by [17] respectively.

$$\mu_0 = F\sigma^2, \sigma_0 = 2F\sigma^4 \tag{10}$$

$$\mu_e = F\sigma^2 + E_n, \sigma_e^2 = 2F\sigma^4 + 4\sigma^2 E_n \tag{11}$$

where E_n is the signal energy within the nth integration period and F is the number of degrees of freedom given by $F = 2BTb + 1$. Here B is the signal bandwidth.

3. TOA Estimation Based on Energy Detector

3.1. TOA Estimation Algorithms

There are many TOA estimation algorithms based on ED for determining the start block of a received signal. The simplest is Maximum Energy Selection (MES), which chooses the maximum energy value to be the start of the signal value. The TOA is estimated as the center of the corresponding integration period:

$$\tau_{MES} = \left[\arg\max_{1 \le n \le N_b} \{ z[n] \} - 0.5 \right] Tb \tag{12}$$

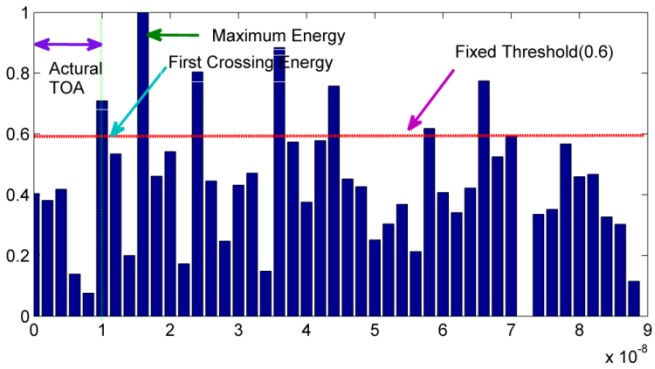

Figure 3. TOA Estimation Based on Energy Detector

However, as show in Figure 3, the maximum energy value may not be the first energy block [13], especially in NLOS environments. On average, the first energy value $z[n]$ is located before the maximum $z[n_{\max}]$, i.e. $n \le n_{\max}$. Thus, Threshold Crossing TOA estimation has been proposed where the received energy values are compared to an appropriate threshold α. In this case, the TOA estimation is given by

$$\tau_{TC} = \left[\arg\min_{1 \le n \le n_{\max}} \{ n \mid z[n] \ge \xi \} - 0.5 \right] Tb \tag{13}$$

It is difficult to determine an appropriate threshold α directly, so usually a normalized threshold α_{norm} is calculated. Using α_{norm}, α is given by

$$\alpha = \alpha_{norm} \left(\max(z(n)) - \min(z(n)) \right) + \min(z(n)) \tag{14}$$

τ_{TC} is then obtained using (13). A simpler Threshold Crossing algorithm is the Fixed Threshold algorithm where the threshold is set to a fixed value, for example α_{norm}=0.4 .The problem in this case becomes one of how to set the threshold. It should be based on the statistics of the signal energy, particularly for multipath, NLOS indoor environments.

3.2. Error Analysis

The Mean Absolute Error (MAE) of TOA estimation based on Threshold Crossing was analyzed, and closed form error expressions derived. The MAE can be used to evaluate

the quality of an algorithm, and is defined as

$$MAE = \frac{1}{N}\sum_{n=1}^{N}\left(t_n - t_n\right) \tag{15}$$

where t_n is the *nth* actual propagation time, $\hat{t}_n$ is the *nth* TOA estimate, and *N* is the number of TOA estimates.

4. Statistical Characteristics

Kurtosis, skewness and standard deviation of the energy blocks are analyzed in this section.

4.1. Kurtosis

The kurtosis is calculated using the second and fourth order moments and is given by:

$$K = \frac{E\left[\left(x_i - \mu_x\right)^4\right]}{E\left[\left(x_i - \mu_x\right)^2\right]^2} = \frac{E\left[\left(x_i - \mu_x\right)^4\right]}{\sigma_x^4} \tag{16}$$

where μ_x is the mean value, and σ_x is the standard deviation. The kurtosis for a standard normal distribution is three. For this reason, kurtosis is often redefined as $K = K - 3$ (often referred to as "excess kurtosis"), so that the standard normal distribution has a kurtosis of zero, positive kurtosis indicates a "peaked" distribution and negative kurtosis indicates a "flat" distribution. For noise only (or for a low SNR) and sufficiently large *F* (degrees of freedom of the Chi-square distribution), $z[n]$ has a Gaussian distribution and kurtosis = 0. On the other hand, as the SNR increases, kurtosis will tend to increase.

4.2. Standard Deviation

The standard deviation is a widely used measure of variability. It shows how much variation or "dispersion" there is from the average (mean or expected value). The standard deviation is given by:

$$D = \sqrt{\frac{\sum_{i=1}^{N}\left(x_i - \mu_x\right)^2}{N-1}} \tag{17}$$

4.3. Skewness

The Skewness is given by:

$$S = \frac{1}{\left(N-1\right)\delta^3}\sum_{i=1}^{N}\left(x_i - \mu_x\right)^3 \tag{18}$$

where μ_x is the mean value, and δ is the standard deviation of the energy values. The skewness for a normal distribution is 0; in fact any symmetric data will have a skewness of zero. Negative values of skewness indicate that the data is skewed left, while positive values indicate data that is skewed right. Skewed left indicates that the left tail is long relative to the right tail, while skewed right indicates the opposite. For noise only (or very low SNR), and sufficiently large *F*, skewness≈0. As the SNR increases, skewness will tend to increase.

4.4. Characteristics of Parameters

In order to examine the characteristics of parameters, the residential LOS and NLOS channel models from the IEEE802.15.3c standard are employed. For each SNR value, 1000 channel realizations are generated and sampled at $f_c = 1 \cdot e^{10} Hz$. The other system

parameters are $T_f = 200ns, T_c = 1ns$, Tb is from 1ns to 4ns and N=1. Each realization has a TOA uniformly distributed within $(0 - T_f)$.

The parameters were calculated, and the results obtained are shown in from Figures 4-11. This results show that the characteristics of the parameters with respect to the SNR are similar for the two channels. Further, from Figures 4-11, the results of the division of two variables (skewness and kurtosis) are used as the new parameter 'S/K'. By the same token, the results of the division of two variables (kurtosis and skewness) are used as the new parameter 'K/S'. We can see that K/S, skewness, kurtosis increases as the SNR increases both in channel CM1.1 and CM2.1, but K/S changes more rapidly in comparison with other parameters. Conversely, the S/K and standard deviation decrease with the increase of the SNR, but the standard deviation changes more rapidly in comparison with other parameters. Since standard deviation and K/S change more rapidly than other parameters, they better reflect changes in SNR, and so they are even more suitable for TOA estimation. Moreover, when the SNR is less than 11 dB, K/S changes slowly while the S/K changes rapidly. On the other hand, when the SNR is higher than 11 dB, the S/K changes rapidly but the K/S changes slowly. Therefore, no single parameter is a good measure of SNR change over a wide range of values. Thus, a joint metric based on skewness, kurtosis and standard deviation is proposed in the next section for TOA estimation. Based on the results, a joint metric for TOA estimation is formulated as:

$$G = K / S - SD \tag{19}$$

where 'K/S' is the results of the division of two variables (kurtosis and skewness) and 'SD' is standard deviation.

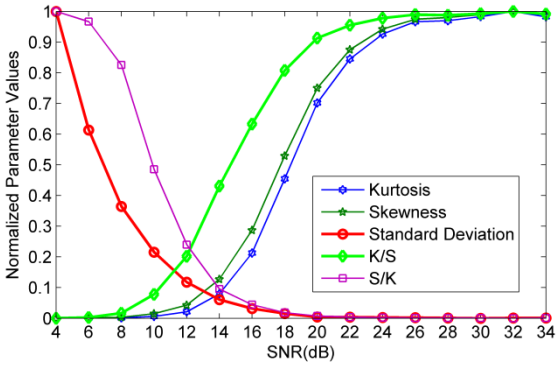

Figure 4. Parameters Change with SNR in CM1.1 with Tb=1ns

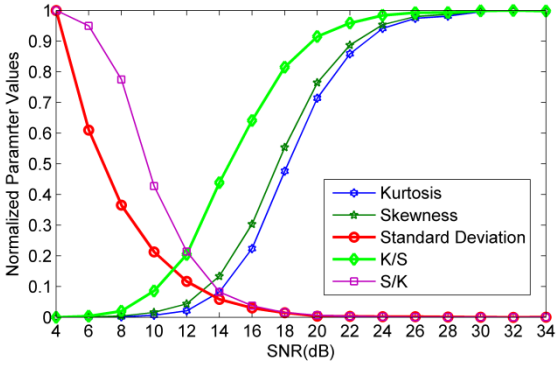

Figure 5. Parameters Change with SNR in CM1.1 with Tb=2ns

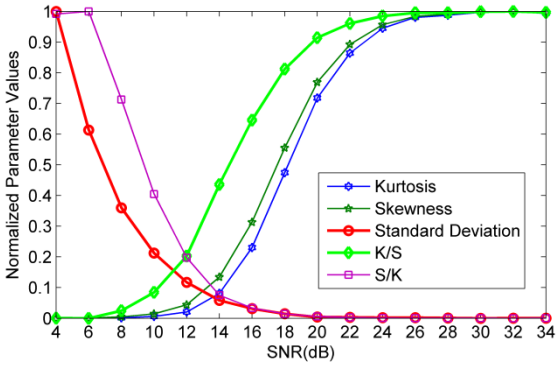

Figure 6. Parameters Change with SNR in CM1.1 with Tb=3ns

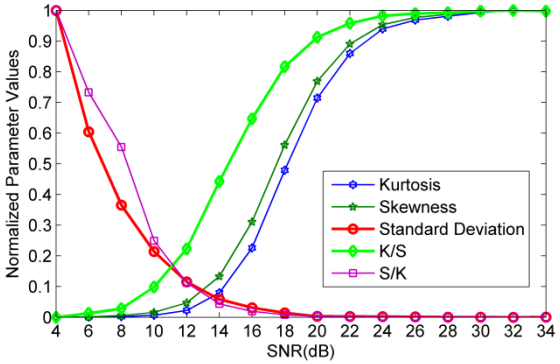

Figure 7. Parameters Change with SNR in CM1.1 with Tb=4ns

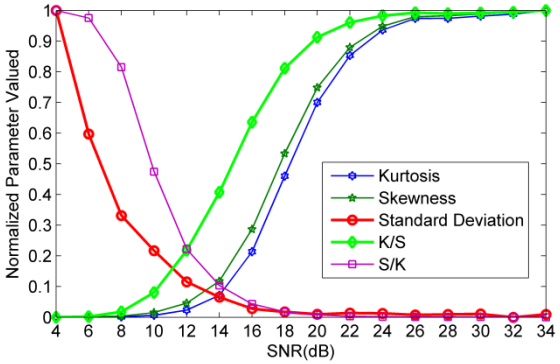

Figure 8. Parameters Change with SNR in CM 2.1 with Tb=1ns

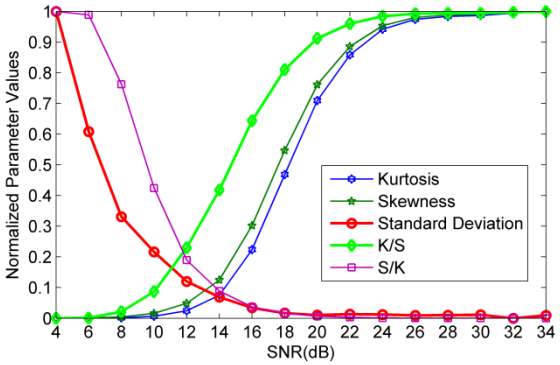

Figure 9. Parameters Change with SNR in CM 2.1 with Tb=2ns

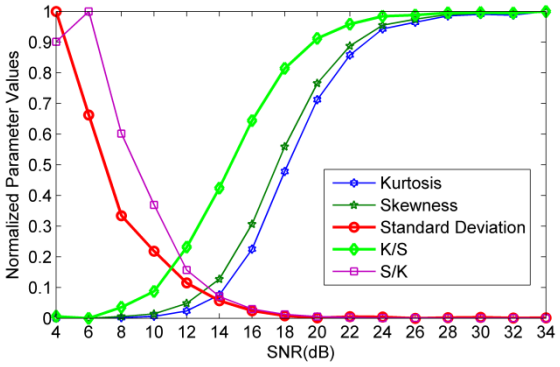

Figure 10. Parameters Change with SNR in CM 2.1 with Tb=3ns

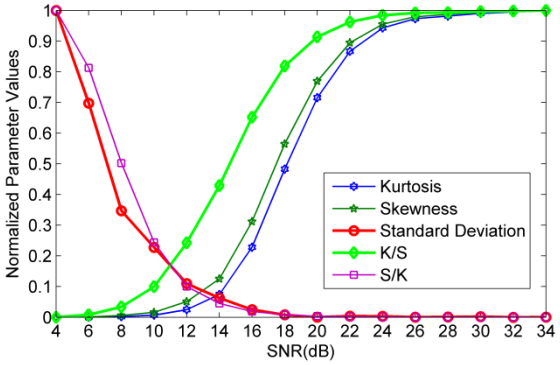

Figure 11. Parameters Change with SNR in CM 2.1 with Tb=4ns

5. Optimal Threshold Selection

Before training the BP-ANN, the relationship between *G* and the optimal normalized threshold α_{opt} must be established. According to Figures 12-13, the curves for CM1.1 and CM2.1 for a given value of *Tb* are similar, so models are derived only for *Tb* = 1ns, *Tb* = 2ns, *Tb* = 3ns and *Tb* = 4ns.The steps to establish the relationship between G and α_{opt} can expressed as:

(1)Generating amounts of channel realizations (1000 channel realizations are generated in this paper) aiming at different channel model (CM1.1 and CM2.1), *Tb* = 1ns, 2ns, 3ns and 4ns, and SNR value in the range from 4 to 34dB.

(2) Calculating the average value of MAE with respect to different α_{norm} for different *G* value, channel model (CM1.1 and CM2.1), and *Tb* as shown in Section"5.2.Relationship between MAE and the Normalized Threshold". In the process of simulation, because of the signals are generated randomly, so there are different MAE values with respect to one normalized threshold, so the average MAE is obtained. At the same time, because *G* is a real value, *G* should be rounded to the nearest discrete value, for example integer value or half-integer value.

(3) Selecting the normalized threshold with the lowest MAE as the best threshold α_{best} with respect to *G* for each channel model and *Tb*, as shown in section "5.3 Optimal Thresholds".

(4) Calculating the average normalized thresholds of channels CM1.1 and CM2.1 for different *G* as the optimal normalized threshold α_{norm}, as shown in section"5.3 Optimal Thresholds".

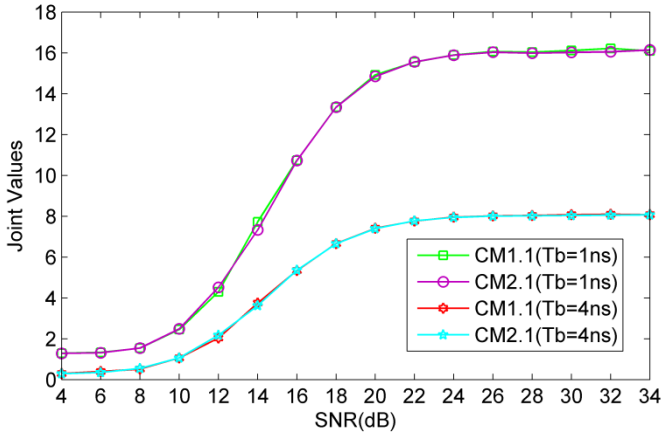

Figure 12. Average Values with Respect to SNR for Different CM and Tb

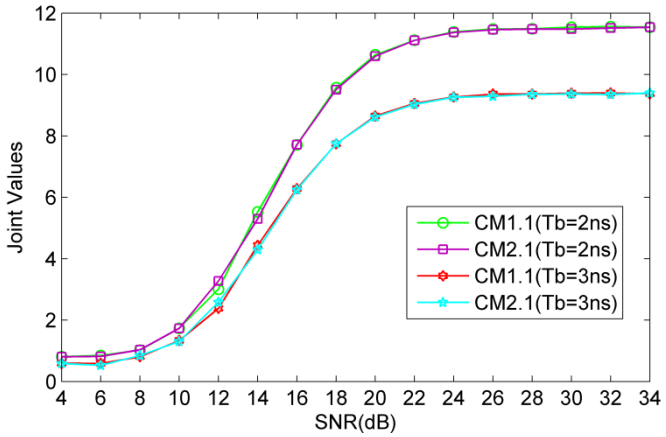

Figure 13. Average Values with Respect to SNR for Different CM and Tb

5.1. Relationship between G and SNR

In order to verify the relationship between the proposed metric *G* and SNR, 1000 channel realizations were generated when SNR is from 4 to 34dB in each IEEE802.15.3c channel. The average values of *G* are presented in the Figures 12-13. The results show that *G* is a monotonic function for a large range of SNR values, and it is even much more sensitive to changes in SNR. The eight fixed curves differ somewhat due to the Channel Model and integration period used. The figure shows that *G* is more sensitive to *Tb*.

5.2. Relationship between MAE and the Normalized Threshold

In order to determine the best threshold (α_{best}) based on G, the relationship between MAE and normalized threshold (α_{norm}) was investigated. 1000 channel realizations with SNR = {4, 5,…, 34} dB were simulated under CM1.1 and CM2.1 environments. α is the threshold which is compared to the energy values to find the first threshold crossing. When α is bigger than $z[n_{\max}]$, we can't get the TOA estimation, so in this case, α is set to be 1.

In the simulation, all *G* values were rounded to the nearest integer and half-integer values for all SNR values. From Figures 14-21 show the relationship between MAE and the Normalized Threshold in the CM1.1 and CM2.1 channels, respectively, with *Tb* is 1ns, 2ns, 3ns and 4ns. The relationship is always that the MAE decreases as *G* increases.

Another conclusion is that the minimum MAE is lower as G increases. The normalized threshold α_{norm} with respect to the minimum MAE is just the best threshold α_{best}. The relationship between α_{best} and G will be shown in the next section.

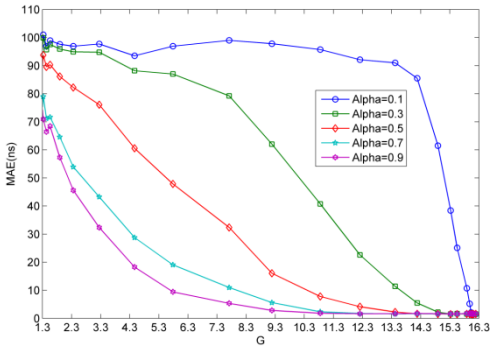

Figure 14. MAE with Respect to G (CM1.1 and Tb=1ns)

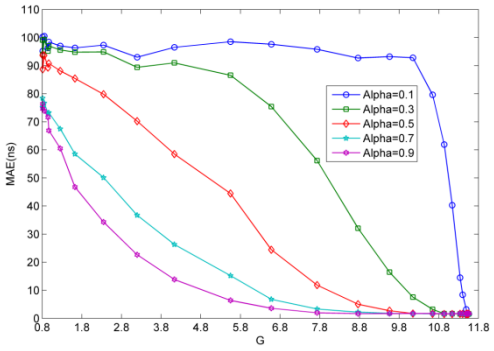

Figure 15. MAE with Respect to G (CM1.1 and Tb=2ns)

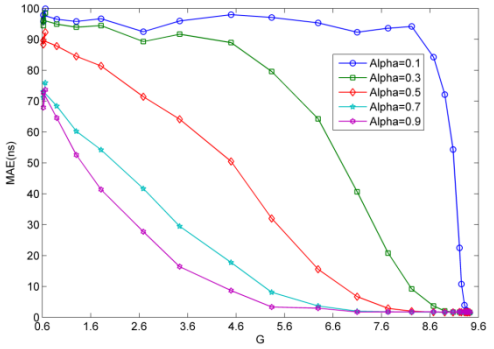

Figure 16. MAE with Respect to G (CM1.1 and Tb=3ns)

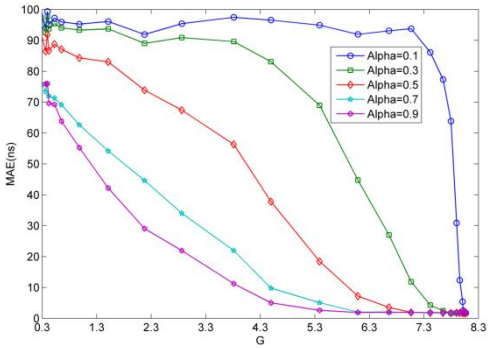

Figure 17. MAE with Respect to G (CM1.1 and Tb=4ns)

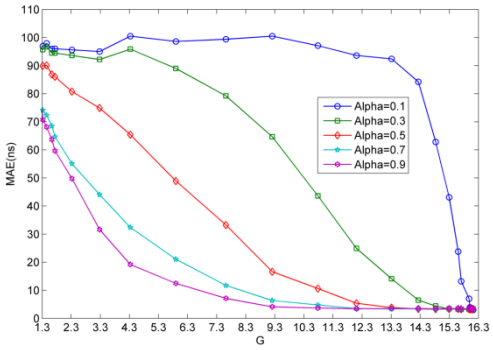

Figure 18. MAE with Respect to G (CM2.1 and Tb=1ns)

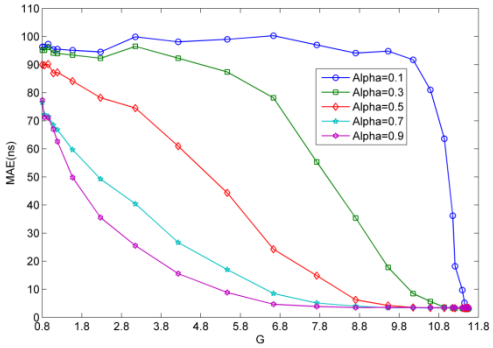

Figure 19. MAE with Respect to G (CM2.1 and Tb=2ns)

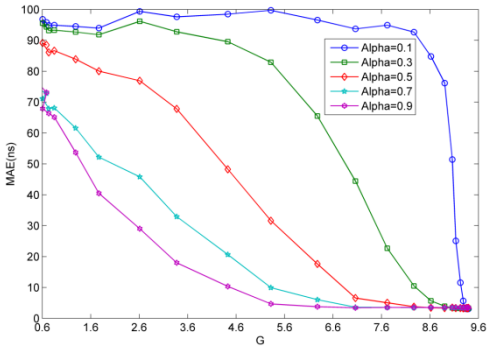

Figure 20. MAE with Respect to G (CM2.1 and Tb=3ns)

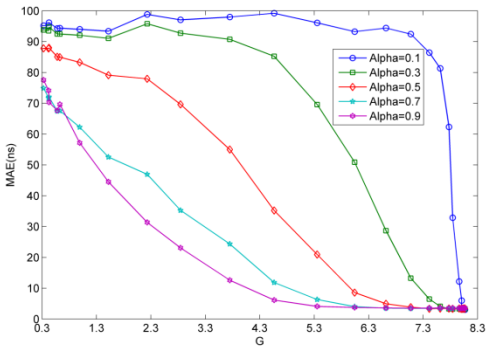

Figure 21. MAE with Respect to G (CM2.1 and Tb=4ns)

5.3. Optimal Thresholds

The normalized threshold α_{norm} with respect to the minimum MAE is called the best threshold α_{best} for a given G. Therefore, the lowest points of the curves in Figures 14-21 for each G are selected as the α_{best}.

These results show that the relationship between the two parameters is not affected significantly by the channel model, but is more dependent on the integration period, so the values for channels CM1.1 and CM2.1 can be combined. Therefore, the average of the two values is used as the optimal normalized threshold

$$\alpha_{opt}^{(Tb=1ns)}(G)=\frac{\alpha_{best}^{(CM1.1,\,Tb=1ns)}(G)+\alpha_{best}^{(CM2.1,\,Tb=1ns)}(G)}{2} \tag{20}$$

$$\alpha_{opt}^{(Tb=2ns)}(G)=\frac{\alpha_{best}^{(CM1.1,\,Tb=2ns)}(G)+\alpha_{best}^{(CM2.1,\,Tb=2ns)}(G)}{2} \tag{21}$$

$$\alpha_{opt}^{(Tb=3ns)}(G)=\frac{\alpha_{best}^{(CM1.1,\,Tb=3ns)}(G)+\alpha_{best}^{(CM2.1,\,Tb=3ns)}(G)}{2} \tag{22}$$

$$\alpha_{opt}^{(Tb=4ns)}(G)=\frac{\alpha_{best}^{(CM1.1,\,Tb=4ns)}(G)+\alpha_{best}^{(CM2.1,\,Tb=4ns)}(G)}{2} \tag{23}$$

6. Threshold Selection Using an BP-ANN based on G

6.1. Structure of the BP-ANN

In this paper, a BP-ANN is used which consists of an input layer, a hidden layer and an output layer, as shown in Figure 22.

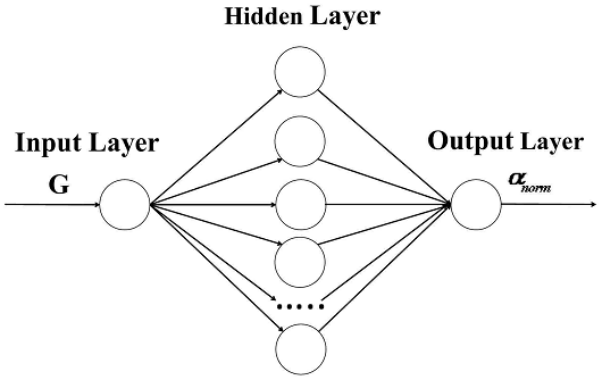

Figure 22. Structure of the BP-ANN

The weights between the layers are adjusted according to the error which is calculated with the value of input and output. Usually, it is difficult to choose the number of neurons in the hidden layer [28]. Several BP-ANNs are initialized and trained and the best one is selected. Moreover, in [29], an algorithm (implemented in Mat lab) for initializing the BP-ANN weights and biases is used, which warrants the stability and convergence at the beginning of the training. For the BP-ANN, the number of neurons in the hidden layer is the key to determine success. The BP-ANN can't get enough information to solve the problem if the neurons are so few in number, at the same time, it will not only increase the training time but also could lead to the "over-fitting" problems if the neurons is so much in number. In [30], the author proposed that the number of neurons can be estimated based on the results that the percentage of the MSE values where the BP-ANN is trained repeatedly, if we use the method, we can get the results as follows

For *Tb* = 1ns, when the number of neurons in the hidden layer is more than 24, the percentage is greater than 95% and changes only slightly with increasing values, so 24 is selected as the number of neurons in the proposed BP-ANN.

For *Tb* = 4ns, when the number of neurons in the hidden layer is more than 20, the percentage is greater than 90% and changes only slightly with increasing values, so 20 is selected as the number of neurons in the proposed BP-ANN.

For *Tb* = 2ns, when the number of neurons in the hidden layer is more than 30, the percentage is greater than 95% and changes only slightly with increasing values, so 30 is selected as the number of neurons in the proposed BP-ANN.

For *Tb* = 3ns, when this number of neurons is more than 20, the percentage is greater than 90% and changes very little with increasing values, so 20 is selected in this case. The results show that the BP-ANN needs too many neurons.

In order to decrease the computational complexity, improve the effectiveness of the model at the same time. In this paper, we propose that it can be estimated based on the results where the BP-ANN is trained repeatedly. Here, the number (save as 'n') of neurons in the hidden layer is varied from 2 to 40, and for each value, the BP-ANN was trained 100 times and the mean squared error (MSE) calculated. When the least MSE < 1e-32 occurred for the first time, now the 'n' value will be referred as the number of neurons. According to the principle, we got the values for *Tb* = 1ns, 2ns, 3ns and 4ns respectively.

For *Tb* = 1ns, when the number of neurons in the hidden layer is 14, the least MSE = 5.8933e-33, so 14 is selected as the number of neurons in the proposed BP-ANN.

For *Tb* = 4ns, when the number of neurons in the hidden layer is 10, the least MSE = 7.8193e-33, so 10 is selected as the number of neurons in the proposed BP-ANN.

For *Tb* = 2ns, when the number of neurons in the hidden layer is 12, the least MSE = 4.6757e-33, so 12 is selected as the number of neurons in the proposed BP-ANN.

For *Tb* = 3ns, when this number of neurons is 12, the least MSE = 7.7639e-33, so 12 is selected as the number of neurons in the proposed BP-ANN.

Because of the value of α_{norm} changes from 0 to 1, here the log-sig function is used as the transfer function between the neurons of both the hidden and output layers. This function (shown in Figure 23) is defined as

$$\log sig(x) = 1 \Big/ \left(1 + e^{(-x)}\right) \tag{24}$$

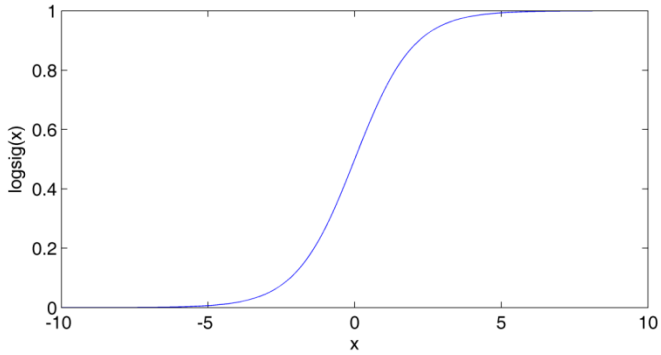

Figure 23. Waveform of Log-sig Function

The Levenberg-Marquardt (LM) algorithm is used in the network training to update the weights and bias values according to LM optimization [12]. Although this algorithm requires more memory than other algorithms, it is often the fastest BP algorithm. Because there is only two input and one output element in the proposed BP-ANN, and only 59 $(\alpha_{norm} - G)$ pairs such as (G = -2 to 16 for Tb = 1ns, G = -2 to 9 for Tb = 4ns, G = 2 to 12 for Tb = 2ns and G = -2 to 10 for Tb = 3ns), the memory requirements are modest. The weights and bias values before training were set to random values uniformly distributed between -1 and 1.

6.2. BP-ANN Training

In order to train the BP-ANN, i.e., so as to determine the relationship between G and the normalized threshold α_{norm}, 1000 channel realizations (both CM1.1 and CM2.1) for different SNR which ranges from 4 to 34dB were generated for both Tb = 1ns, 2ns, 3ns and 4ns. These best and the optimal thresholds are given in Figures 24-27.

The integer G values which are in the range from -2 to 16 for Tb = 1ns, from -2 to 9 for Tb = 4ns, from -2 to 12 for Tb = 2ns and from -2 to 10 for Tb = 3ns respectively, were used for training the BP-ANN. Thus, 59 samples which can be used to train the BP-ANN. The results of the training are given in Figures 24-27. The results show that the training results are highly consistent with the optimal values.

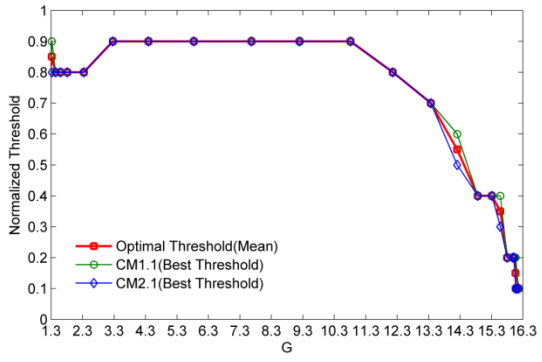

Figure 24. Normalized Threshold with Respect to G for Tb = 1ns

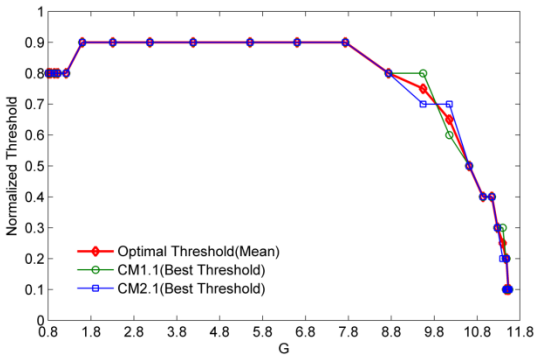

Figure 25. Normalized Threshold with Respect to G for Tb = 2ns

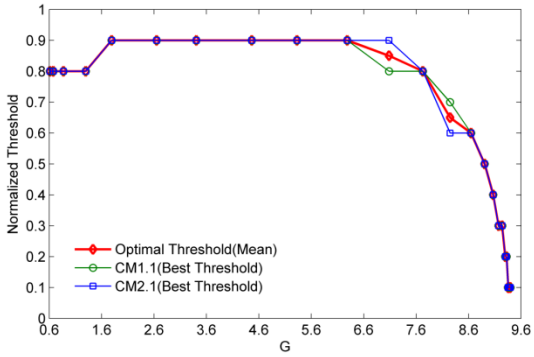

Figure 26. Normalized Threshold with Respect to G for Tb = 3ns

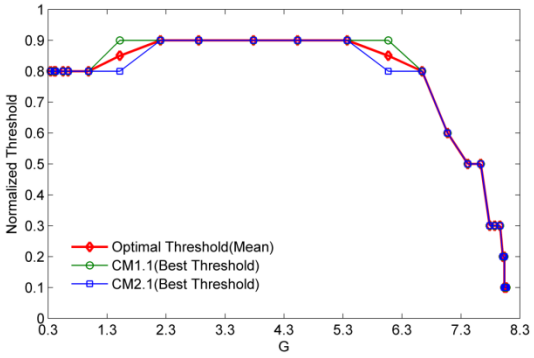

Figure 27. Normalized Threshold with Respect to G for Tb = 4ns

To obtain the best BP-ANN, 1000 separate training iterations were conducted for each value of Tb, and the one with the lowest MSE was selected. The weights from the input layer to the hidden layer is expressed as net-IW{1,1}, the weights from the hidden layer to the output layer is expressed as net-LW{2,1}, the bias of the Hidden is expressed as net-b{1,1}, the bias of the output layer is expressed as net-b{2,1}.

For *Tb* = 1ns, these values are shown in Table 2 and net-b {2, 1} = 3.5663.

Table2. Values for BP-ANN with Tb=1ns

net-IW{1,1}	net-b{1,1}	net-LW{2,1}
5.8005	-68.2990	-0.4554
4.0777	-63.9141	-0.8457
6.1921	-57.5702	-1.3275
0.6873	-13.4278	-19.0302
5.1047	-45.5404	-0.4362
-4.2644	39.5080	-1.2262
4.3202	-33.4983	-0.3966
4.6393	-27.4282	-0.8519
-4.0690	21.5006	-0.0534
4.7626	-15.2362	-0.0004
4.6394	-9.2029	-0.0684
-3.6226	3.9930	-0.8975
4.3695	2.6759	-0.0204
-2.9383	-9.4002	-0.0997

For *Tb* = 2ns, these values are shown in Table3 and net-b {2, 1} = 2.0321.

Table 3. Values for BP-ANN with Tb=2ns

net-IW{1,1}	net-b{1,1}	net-LW{2,1}
-0.3868	57.9682	-1.3818
-3.5581	51.6003	-0.8652
5.4587	-45.3184	-1.0436
-3.7578	39.4027	0.0007
3.7827	-33.3256	0.0734
4.0668	-27.0780	-0.7625
3.4254	-21.2794	0.5641
-5.2345	15.0387	-4.4758
-7.9289	12.0915	-3.5778
-1.3321	2.2401	14.5626
-2.5798	-0.1240	-4.0139
1.8870	11.0232	-0.8140

For *Tb* = 3ns, these values are shown in Table 4 and net-b {2, 1} = 0.1234.

Table 4. Values for BP-ANN with Tb=3ns

net-IW{1,1}	net-b{1,1}	net-LW{2,1}
5.7136	-56.0121	1.6769
5.4211	-50.0108	-3.1470
5.4373	-43.8197	-0.7384
-6.2429	37.5705	1.6481
-2.8596	31.9961	-1.3231
3.6486	-25.7840	0.5971
-4.9526	19.5147	0.8205
-5.8822	13.0604	-0.0106
8.4333	-5.0479	1.7640
4.7439	-1.9152	-1.0851
5.3488	5.3461	0.2573
-5.5439	-11.2284	0.2728

For *Tb* = 4ns, these values are shown in Table 5 and net-b {2, 1} = 0.9657.

Table 5. Values for BPANN with Tb=4ns

net-IW{1,1}	net-b{1,1}	net-LW{2,1}
-3.6870	45.9698	1.6983
7.3102	-58.9964	-7.7206
-5.8579	42.2120	3.8549
4.7416	-27.8132	-1.2339
2.3309	-18.5364	10.3220
9.1378	-36.8516	-1.0893
9.7490	-5.9515	-2.0152
-11.3116	7.1704	-2.8230
-4.9815	-3.8726	-0.0043
2.7654	11.3404	-0.3750

On the other hand, the half integer *G* values in the range from -1.5 to 15.5 for *Tb* = 1ns, from -1.5 to 8.5 for *Tb* = 4ns, from -1.5 to 11.5 for *Tb* = 2ns and from -1.5 to 9.5 for *Tb* = 3ns respectively, were used to conduct the external validation for the trained BPANN.

6.3. Validation of the BP-ANN

In order to evaluate the performance of the trained BP-ANN, the internal validation and external validation were conducted. The *G* values from −2 to 16 for the internal validation, from −1.5 to 15.5 for the external validation with *Tb* = 1ns, from −2 to 12 for the internal validation, from −1.5 to 11.5 for the external validation with *Tb* = 2ns, from −2 to 10 for the internal validation, from −1.5 to 9.5 for the external validation with *Tb* = 3ns, from −2 to 9 for the internal validation, from −1.5 to 8.5 for the external validation with *Tb* = 4ns were input to the BP-ANN to get the estimated normalized thresholds. As shown in Figures 28-35, the four MSEs of the external validation for *Tb* = 1ns, 2ns, 3ns and 4ns are 5.2622e-5, 5.825e-4 1.732e-4 and 4.5311e-4, so the trained BP-ANN output fits well with the optimal normalized thresholds for *Tb* = 1ns, 2ns, 3ns and 4ns. So we believe that the BP-ANN is able to provide values for any *G*, and not just discrete values. The BP-ANN also eliminates the complicated and time consuming optimization process used in Section "Optimal normalized threshold with respect to *G*". The IEEE802.15.3c channel models reflect the statistical properties in specific environments, and the choice of BP-ANN parameters depends on the characteristics of the channel. Our BP-ANN can easily be employed with any channel, and the parameters adjusted to fit any environment. This is particularly useful when the channel is not static.

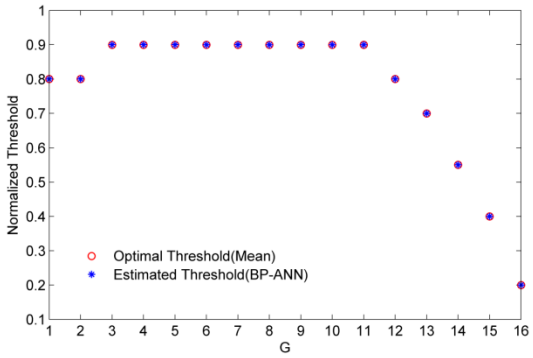

Figure 28. Internal Validation for Tb=1ns

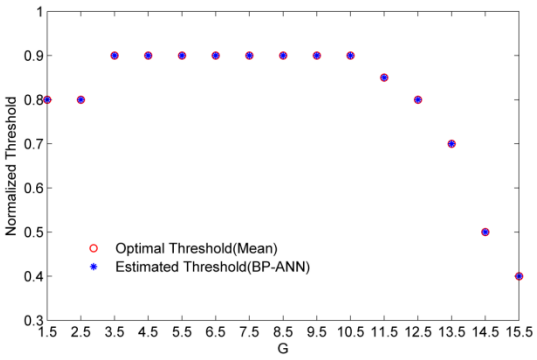

Figure 29. External Validation for Tb=1ns

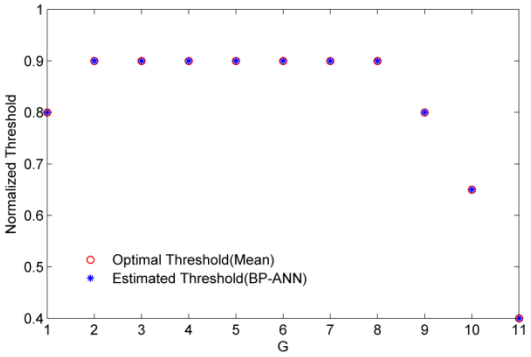

Figure 30. Internal Validation for Tb=2ns

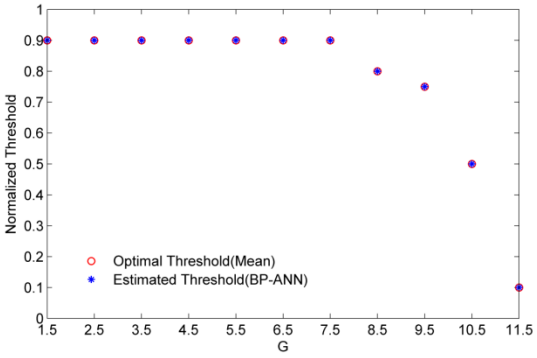

Figure 31. External Validation for Tb=2ns

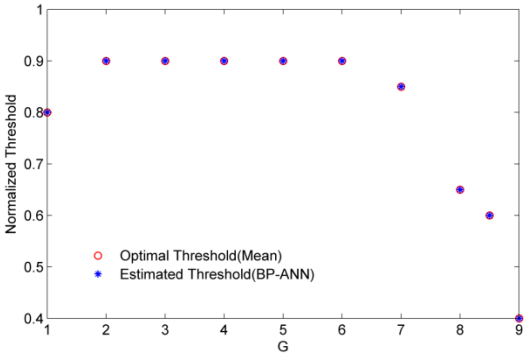

Figure 32. Internal Validation for Tb=3ns

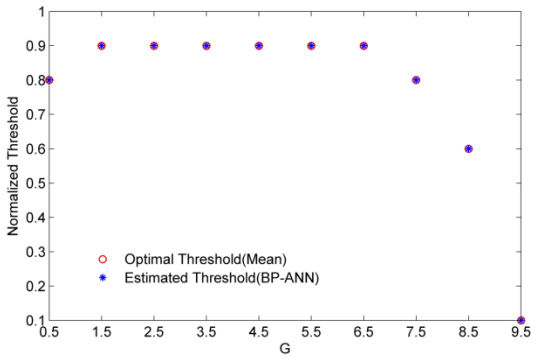

Figure 33. External Validation for Tb=3ns

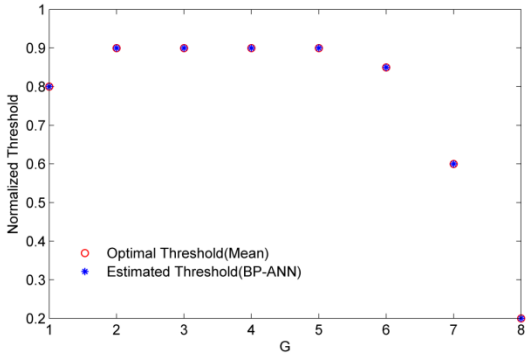

Figure 34. Internal Validation for Tb=4ns

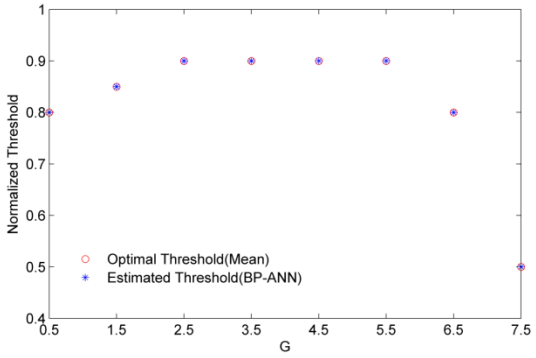

Figure 35. External Validation for Tb=4ns

7. Results and Discussion

In this section, the MAE is examined for different TOA estimation algorithms which based on ED in the IEEE 802.15.3c CM1.1 and CM2.1 channels. As before, 1000 channel realizations are generated for each case. A 2PPM-TH 60 GHz signal is employed, and the received signal is sampled at $f_c = 1 \cdot e^{10}$ Hz. The other system parameters are $T_f = 200ns, T_c = 1ns$ the value of *Tb* is from 1ns to 4ns and *N* = 1. Each realization has a TOA uniformly distributed within $(0 - T_f)$.

The MAE for SNR values from 4dB to 34dB in LOS (CM1.1) is presented in the Figure 36 and Figure 37. At the same time, The MAE for SNR values from 4 dB to 34 dB in NLOS (CM2.1) is presented in the Figure 38 and Figure 39. This shows that the proposed algorithm performs even much better than other algorithm such as MES and FT.

The performance in CM1.1 is better than in CM2.1 aiming at the same *Tb*. In most cases, the performance with $Tb = 1ns$ is better than that with $Tb = [2ns, 3ns \text{ and } 4ns]$ regardless of the channel. The MAE performance with three TOA algorithms in channels CM1.1 and CM2.1 are shown in Figures 36-39 respectively. Here "MES" is the Maximum Energy Selection algorithm, and the normalized threshold for the Fixed Threshold algorithm is set to 0.4 and 0.6. The MAE with the proposed algorithm is lower than other algorithms, particularly at low to moderate SNR values. The proposed algorithm is better except when the SNR is greater than 19 dB. The performance of the proposed algorithm is more robust than the other algorithms, as the performance difference is very small compared to the difference with other algorithms. For almost all SNR values the proposed algorithm is even much better. Conversely, the performance of other algorithms varies greatly and is very bad for low to moderate SNR values.

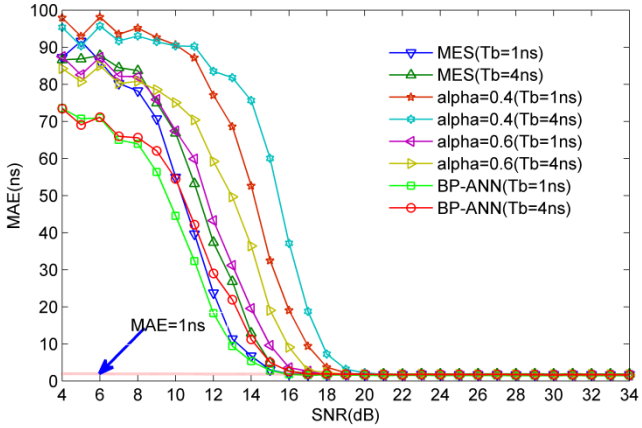

Figure 36. MAE for Different Algorithms with CM1.1 (Tb=1ns and 4ns)

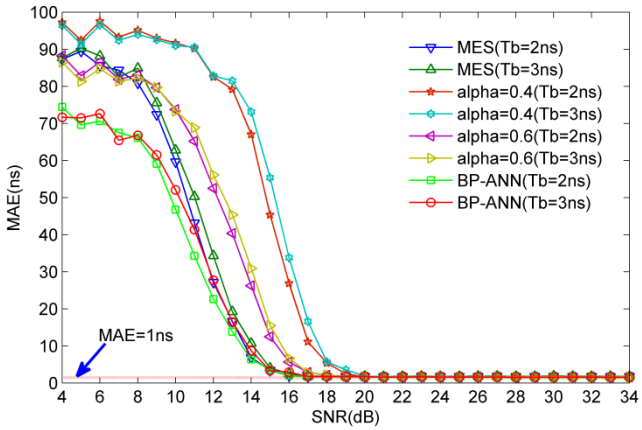

Figure 37. MAE for Different Algorithms with CM1.1 (Tb=2ns and 3ns)

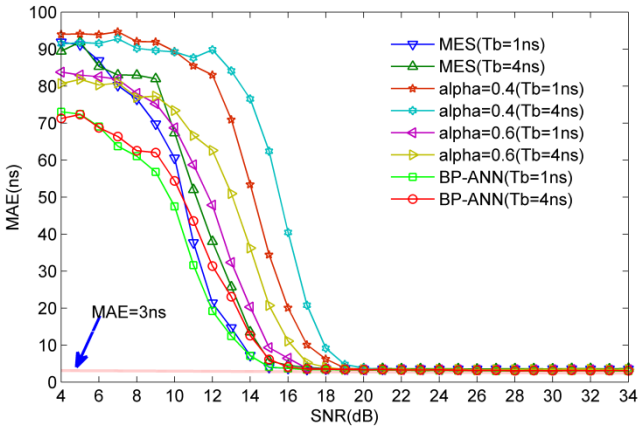

Figure 38. MAE for Different Algorithms with CM2.1 (Tb=1ns and 4ns)

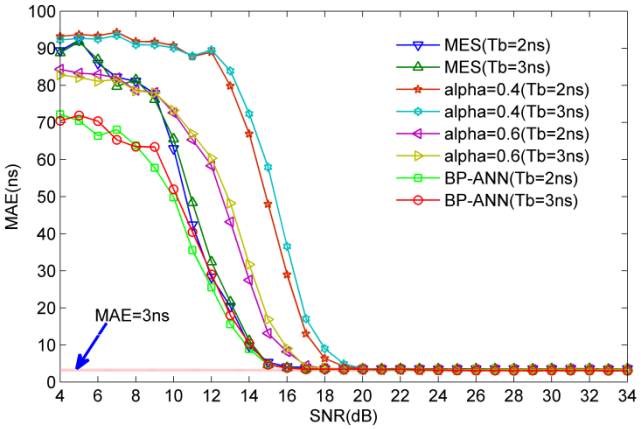

Figure 39. MAE for Different Algorithms with CM2.1 (Tb=2ns and 3ns)

8. Conclusions

Low complex BP-ANN TOA estimation algorithms that based on ED have been examined for IR-60 GHz ranging, positioning, and tracking applications. Statistical parameters were investigated and a joint metric based on kurtosis, skewness and standard deviation was developed for Threshold Crossing TOA estimation according to the results obtained. The best normalized threshold was determined using simulation with the CM1.1 and CM2.1 channels. The effects of the integration period and channel model were investigated. It was determined that the proposed threshold selection technique is largely independent of the channel model. The performance of the proposed algorithm was shown to be better than several known algorithms. In addition, the proposed algorithm is more robust to changes in the SNR and integration period.

Acknowledgments

The authors would like to thank colleagues from the UWB Laboratory in the College of Information Science and Engineering, Ocean University of China, for help with obtaining the measurement data. This work was supported by the Nature Science Foundation of China under Grant No. 60902005, the Qingdao International Science and Technology Cooperation Projects of Qingdao under Grant No. 12-1-4-137-hz, the Nature Science Foundation of China under Grant No. 61301139, the Nature Science Foundation of

Shandong Province No. ZR2014FL014, the Science and Technology Project in Colleges and Universities of Shandong Province No.J14LN53, the Project of Basic Research Application of Qingdao City No. 14-2-4-37-jch and the Project of Basic Research Application of Qingdao City No. 14-2-4-83-jch.

References

[1] L. Zhang, "A fully integrated 60GHz five channel CMOS receiver with 7GHz ultra-wide band width for IEEE 802.11ad standard", Communication, China, vol. 11, no. 6, **(2014)**, pp. 42-50.
[2] S. K. Yong and C. C. Chong, "An overview of multi gigabit wireless through millimeter Wave Strategy: Potentials and Technical Challenges", EURASIP J. Wireless Communications and Networking, vol. 2007, no. 1, **(2007)**, pp. 1-10.
[3] R. C. Daniels and R. W. Heath, "60 GHz wireless communications: emerging requirements and design recommendations", IEEE Vehicular Strategy Society, vol. 2, **(2007)**, pp. 41-50.
[4] C. C. Chong, F. M. Peter, Smulders, et al, "60GHz-Millimeter-Wave Radio Principle, Strategy, and News Results", EURASIP Journal on Wireless Communications and Networking, vol. 2007, no. 1, **(2007)**, pp. 1-8.
[5] S. K. Yong, P. F. Xia P F and Alberto V G, "60-GHz Strategy for Gbps WLAN and WPAN: From Theory to Practice", Beijing: Press of China Machine, **(2013)**.
[6] R. C. Daniels and R. W. Health, "60 GHz wireless communications: emerging requirements and design recommendations", IEEE Vehicular Strategy Magazine, vol. 2, no. 3, **(2007)**, pp. 41-50.
[7] D. Jie, X. Cui, H. Zhang, and G. Wang, "An ultra-wideband location algorithm based on neural network". International Conference on Wireless Communications Networking and Mobile Computing (WiCOM), vol. 11, no. 6, (**2010)**, pp. 56-64.
[8] X. Tu, H. Zhang, X. Cui and T. A. Gulliver, "3D TDOA/AOA location based on extended Kalman filter", International Symposium on Antennas, Propagation and EM Theory (ISAPE), vol. 11, no. 6, (**2010)**, pp. 56-64.
[9] Z. Sahinoglu and S. Gezici, "Ranging in the IEEE 802.15.4a standard", in IEEE Wireless and Microwave Strategy Conference (WAMICON), **(2006)**.
[10] D. Dardari, A. Conti, U. Ferner, A. Giorgetti, and M. Z. Win, "Ranging with ultra-wide bandwidth signals in multipath environments", Proceedings of the IEEE, vol. 97, no. 2, (**2009)**, pp. 404-426.
[11] Y. Zhang, A. K. Brown, W. Q. Malik, and D. J. Edwards, "High resolution 3D angle of arrival determination for indoor UWB multipath propagation", IEEE Transactions on Wireless Communications, vol. 7, no. 8, (**2010)**, pp. 3047-3055.
[12] D. Dardari, A. Giorgetti, and M.Z. Win. "Time of arrival estimation of UWB signals in the presence of narrowband and wideband interference", IEEE International Conference on Ultra-Wideband (ICUWB), **(2007)**.
[13] M. Bocquet, C. Loyez, and A. BenlarbiDelai, " Using enhanced TDOA measurement for indoor localization", IEEE Microwave and WireleSG Components Letters, vol. 15, no.10, (**2005)**, pp. 612-614.
[14] A. Abbasi and M.H. Kahaei, "Improving source localization in LOS and NLOS multipath environments for UWB signals". International CSI Computer Conference (CSICC), **(2009)**.
[15] I. Guvenc and Z. Sahinoglu, "Multi-scale energy products for TOA estimation in IRUWB systems", IEEE Global Telecommunications Conference, (GLOBECOM), **(2005)**.
[16] A. Y. Z. Xu, E. K. S. Au, A. K.S. Wong, and Q. Wang, "A novel threshold based coherent TOA estimation for IR-UWB systems", IEEE Transactions on Vehicular Strategy, vol. 58, no. 8, **(2009)**, pp. 4675-4681.
[17] I. Guvenc and Z. Sahinoglu, "Threshold selection for UWB TOA estimation based on kurtosis analysis", IEEE Communications Letters, vol. 9, no. 12, **(2005)**, pp. 1025-1027.
[18] I. Guvenc and Z. Sahinoglu. "Threshold based TOA estimation for impulse radio UWB systems", IEEE International Conference on Ultra-Wideband, **(2005)**.
[19] "IEEE Standard for Information strategy--Local and metropolitan area networks--Specific requirements--Part 15.3: Wireless Medium Access Control (MAC) and Physical Layer (PHY) Specifications for High Rate Wireless Personal Area Networks (WPAN) amendment 2: millimeter-wave-based alternative physical layer extension". IEEE Computer Society, IEEE 802.15.06-0474-00-003c. New York, USA, **(2009)**
[20] "802.11n-2009-IEEE Standard for Information strategy-- Local and metropolitan area networks--Specific requirements--Part 11: Wireless LAN Medium Access Control (MAC) and Physical Layer (PHY) Specifications Amendment 5: Enhancements for Higher Throughput", IEEE Computer Society, IEEE 978-0-7381-6731-2. New York, USA, **(2009)**.
[21] C. R. Andersonn and T. S. Rappaport, "In-building wideband partition loss measurements at 2.5 and 60GHz", IEEE Transactions on Wireless Communications, vol. 3, no. 3, **(2004)**, pp. 922-928.
[22] S. Collong, G. Zaharia and G. E. Zein, "Influence of the human activity on wide-band characteristics of the 60GHz indoor radio channel", IEEE Transactions on Wireless Communications, vol. 3, no. 6, **(2005)**, pp. 2396-2406
[23] A. Maltsev, R. Maslennikov and A. Sevastyanov, "Experimental investigations of 60GHz WLAN

systems in office environment", IEEE Journal on Selected Areas in Communications, vol. 27, no. 8, **(2009)**, pp. 1488-1499.
[24] M. G. Sanchez, A. V. Alejos and I. Cuinas, "Comparision of space diversity performance in indoor radio channels at 40GHz and 60GHz", Proc. of European Conference on Wireless Strategy, Amsterdam, **(2008)**.
[25] H. B. Yang, "Channel characteristics and transmission performance for various channel configurations at 60GHz", EURASIP Journal on Wireless Communications and Networking, vol. 2007, no. 1, **(2007)**, pp. 43-43.
[26] N. Li, "Study on the properties of 60 GHz impulse radio communication system". Qingdao: Ocean University of China, **(2012)**.
[27] X. Cui, C. Wu and J. Li, "UWB simulation of energy detection algorithm based on the Internet of things", Application of micro-computer, vol, 27, no. 9, **(2011)**, pp.20-26.
[28] S. Haykin, Neural Networks: A Comprehensive Foundation, 2nd edn. (Prentice-Hall, London, 1999)
[29] R. Vicen-Bueno, R. Carrasco-Alvarez, M. Rosa-Zurera, J.C. Nieto-Borge, M.P. Jarabo-Amores, Artificial neural network-based clutter reduction systems for ship size estimation in maritime radars. EURASIP Journal Advances in Signal Processing 2010, 1 – 15 (2010). 10.1155/2010/380473
[30] Hao Zhang, Xuerong Cui and T Aaron Gulliver. Remotely-sensed TOA interpretation of synthetic UWB based on neural networks, EURASIP Journal on Advances in Signal Processing, vol. 2012, **(2012)**.

Authors

Xiaolin Liang, He now studies in the College of Information Science and Engineering and is a PhD candidate in the Ocean University of China. His research interests include ultra-wideband radio systems, 60GHz wireless communication system.

Tingting Lv, She received the PhD degree in the College of Information Science and Engineering from the Ocean University of China in 2013. She is now a lecture in the College of Information Science and Engineering. Her research interests include ultra-wideband radio systems, 60GHz wireless communication system.

Hao Zhang, He received the MBA degree in the New York Institute of Technology, American in 2001 and the PhD degree in the Electrical and Computer Engineering from the University of Victoria, Canada in 2004. He was a project manager for the Microsoft Inc. in the United States during January-May 2000. During 2004-2008, he was the vice president for the United States Gamma Capital Inc. He is now an adjunct assistant professor in the Department of Electrical and Computer Engineering. Also he becomes a professor and the PhD supervisor in the College of Information Science and Engineering from the Ocean University of China in 2006. His research concerns ultra-wideband radio systems, 60GHz wireless communication system and MIMO wireless communication.

T. Aaron Gulliver received the PhD degree in the Electrical and Computer Engineering from the University of Victoria, Canada in 1989. He is now a professor and the PhD supervisor in the Department of Electrical and Computer Engineering. In 2002, he becomes a Fellow of the Engineering Institute of Canada, and in 2012 a Fellow of the Canadian Academy of Engineering. He is also a senior member of IEEE. His research concerns information theory and communication theory, algebraic coding theory and smart grid and UWB communication.